Local symmetries in liquid $Al_{60}Mn_{40}$ and $Al_{71}Pd_{19}Mn_{10}$ alloys

1994 J. Phys.: Condens. Matter 6 5791

(http://iopscience.iop.org/0953-8984/6/30/003)

J. Phys.: Condens. Matter 6 (1994) 5791–5804. Printed in the UK

Local symmetries in liquid $Al_{60}Mn_{40}$ and $Al_{71}Pd_{19}Mn_{10}$ alloys

M Maret†§, F Lançon‡ and L Billard‡

† Laboratoire de Thermodynamique et Physico-Chimie Métallurgiques, CNRS URA 29, ENSEEG, BP75, 38402 St Martin d'Hères Cédex, France

‡ Département de Recherche Fondamentale sur la Matière Condensée, CEA, SP2M/MP, 38054 Grenoble Cédex 9, France

Received 21 February 1994, in final form 18 April 1994

Abstract. The local symmetries in the liquid $Al_{60}Mn_{40}$ and $Al_{71}Pd_{19}Mn_{10}$ alloys were characterized in terms of the Voronoï polyhedra built in the three-dimensional configurations generated by the molecular dynamics and/or reverse Monte Carlo methods. Comparison with the liquid $Al_{80}Mn_{20}$, previously studied, shows that the topological ordering pointed out in the $S_{NN}(q)$ functions of these three liquid alloys is basically grounded on the same types of local symmetry. However, from a finer analysis, it turns out that the two quasicrystal-forming liquids $Al_{80}Mn_{20}$ and $Al_{71}Pd_{19}Mn_{10}$ are structurally closer.

1. Introduction

The existence of a premonitory local icosahedral order in the $Al_{80}Mn_{20}$ quasicrystal-forming liquid was shown via the construction of the Voronoï polyhedra in the three-dimensional particle configurations generated by both molecular dynamics (MD) and reverse Monte Carlo (RMC) simulations (Maret *et al* 1993b, hereafter referred to as I). The importance of such local symmetry was given by the percentage of the pentagonal dodecahedra found, equal to 2.3% in the MD configurations and 1% in the RMC ones. Since the agreement between the experimental pair correlation functions $g_{ij}(r)$ and those calculated from the simulated liquid configurations was clearly better using the RMC method, the value of 1% is probably closer to the real amount of icosahedral order. Without referring to other liquid alloys, this percentage seems very small. However, the same analysis applied to the liquid $Al_{80}Ni_{20}$ yielded a percentage of pentagonal dodecahedra twenty times smaller than in $Al_{80}Mn_{20}$ whatever the simulation method used. Since in contrast with $Al_{80}Mn_{20}$, the liquid $Al_{80}Ni_{20}$ forms no quasicrystal and exhibits a number–number structure factor $S_{NN}(q)$ without any sign of local icosahedral order (Maret *et al* 1990), it was concluded that local icosahedral order was a relevant feature to liquid $Al_{80}Mn_{20}$. To complete this study, we present in this paper the analysis of local symmetries in two other Al-based liquid alloys whose local structure has already been studied by neutron diffraction using isomorphous substitution between Mn atoms and an equiatomic mixture of FeCr atoms.

(i) The first one is the alloy $Al_{60}Mn_{40}$ for which the three $g_{ij}(r)$ functions were determined (Maret *et al* 1991). Despite the fact that this alloy falls outside the quasicrystal-forming composition range, its $S_{NN}(q)$ function exhibits signs of icosahedral ordering,

§ Present address: Institut de Physique et Chimie des Matériaux de Strasbourg, Groupe GEMME, UMR 46, 23 rue du Loess, 67037 Strasbourg, France.

0953-8984/94/305791+14$19.50

i.e. a sharp first peak and a second peak that tends to form a double-component peak at positions $1.7q_1$ and $2q_1$ (q_1 being the first peak position). As for $Al_{80}Mn_{20}$ both MD and RMC methods are applied to $Al_{60}Mn_{40}$. For molecular dynamics simulations, we need effective interatomic potentials which have been extracted from diffraction data using an approximation of classical liquid theory (the Percus–Yevick approximation). On the other hand, to test the sensitivity of the reverse Monte Carlo method to the chosen initial configuration and to the $g_{ij}(r)$ reference functions, a comparison of the statistics of the Voronoï polyhedra obtained in the different corresponding equilibrium configurations will be presented.

(ii) The second liquid is the ternary alloy $Al_{71}Pd_{19}Mn_{10}$ which forms a perfect icosahedral quasicrystal on slow cooling (Tsai *et al* 1990). One of the most interesting neutron diffraction results was that the $S_{NN}(q)$ function of this liquid, measurable by the structure factor of the alloy $Al_{71}Pd_{19}[Mn_{0.25}(FeCr)_{0.75}]_{10}$, superimposed very well on the $S_{NN}(q)$ function of liquid $Al_{80}Mn_{20}$ as plotted as a function of q/q_1 (Maret *et al* 1993a), suggesting a similarity between the two liquid alloys. However, since only three combinations, MnMn, MnA and AA, of the six functions $g_{ij}(r)$ necessary for a complete knowledge of its structure were determined in a pseudo-binary $A_{90}Mn_{10}$ (A=Al or Pd) description, the extraction of effective interatomic potentials from these data was not attempted. Therefore, only RMC simulations are performed based on these combinations of partial functions.

2. Molecular dynamics simulations of liquid $Al_{60}Mn_{40}$

2.1. Procedure and interatomic potentials

The molecular dynamics simulations were performed for a cubic cell containing 518 Al atoms and 346 Mn atoms with periodic boundary conditions at constant volume and constant temperature ($T = 1500$ K, about 30 K above the liquidus line). The edge of the box, a_0, is adjusted such that the atomic density, n, is equal to that of the liquid ($a_0 = 23.8$ Å for $n = 0.064$ atoms Å^{-3}). In the starting configuration, the atomic positions are randomly chosen with the constraint of a minimal distance equal to 2.2 Å for AlAl pairs and 2.1 Å for AlMn and MnMn pairs. Based on a constrained dynamics method (Hoover *et al* 1982), the motions of particles are governed through the effective interatomic potentials, $\phi_{ij}(r)$, deduced from our diffraction data (Maret *et al* 1991).

As for the composition $Al_{80}Mn_{20}$, we use the Percus–Yevick approximation expressed as

$$\phi_{ij}(r) = k_B T \ln[1 - C_{ij}(r)/g_{ij}(r)]. \tag{1}$$

The direct correlation functions $C_{ij}(r)$ were calculated by Fourier transformation of the functions $\tilde{C}_{ij}(q)$ which are related to the experimental Ashcroft–Langreth partial structure factors $S_{ij}(q)$. As was emphasized for $Al_{80}Mn_{20}$ in paper I, the interatomic potentials are sensitive to the low-q parts of $\tilde{C}_{ij}(q)$, therefore we must find a way to extrapolate the $S_{ij}(q)$ functions down to the long-wavelength limits. By relying on previous results on the small-angle scattering behaviour of liquid Na (Matthai and March 1982), the low-q parts of the three total structure factors used for the determination of the three $S_{ij}(q)$ factors are expressed as follows:

$$S(q) = S(0) + a_1 q + a_2 q^2. \tag{2}$$

The limits $S(0)$ are calculated from the thermodynamic quantities (Maret *et al* 1991) and the coefficients a_j are deduced from a relatively good fit of the experimental $S(q)$ function

between 0.3 and 0.8 Å^{-1}. From the expression (2), we can calculate the $S_{ij}(q)$ factors and then the $\tilde{C}_{ij}(q)$ down to 0.

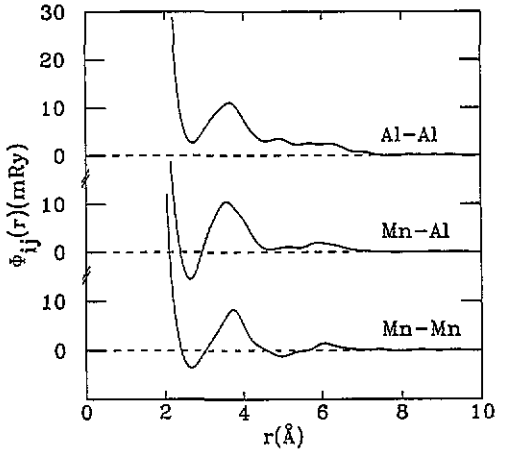

Figure 1. Effective interatomic potentials $\phi_{ij}(r)$ derived from diffraction data for liquid $Al_{60}Mn_{40}$.

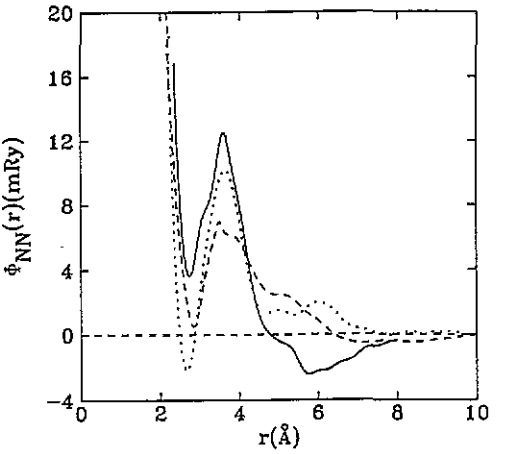

Figure 2. Mean interatomic potential $\phi_{NN}(r)$ derived from diffraction data for liquid $Al_{80}Mn_{20}$ (—), $Al_{60}Mn_{40}$ (. . .) and $Al_{80}Ni_{20}$ (- - -).

The three effective interatomic potentials deduced from (1) are shown in figure 1; all of them exhibit after the main minimum a marked maximum located in the region between the first- and the second-neighbour distances. It is interesting to mention the existence of such a maximum in the special form of pair potential proposed by Dzugutov (1992) for yielding icosahedral local order in a simple monatomic liquid. For a relevant comparison, the mean interatomic potential $\phi_{NN}(r)$ of the binary liquid $Al_{60}Mn_{40}$ is calculated from the three $\phi_{ij}(r)$ potentials as follows:

$$\phi_{NN}(r) = c_1^2\phi_{11}(r) + c_2^2\phi_{22}(r) + 2c_1c_2\phi_{12}(r). \tag{3}$$

The potential $\phi_{NN}(r)$ is shown in figure 2 together with those corresponding to the two other liquid alloys previously studied, $Al_{80}Mn_{20}$ and $Al_{80}Ni_{20}$, using the data published in paper I. It appears that the height of the first maximum increases with the quasicrystal-forming ability, and the ratio of its position to the first minimum position is close to 1.3, i.e. midway between the first two distances in the icosahedral polytope {3, 3, 5} equal to 1 and 1.7 on the scale of the first interatomic distance (Sadoc and Mosseri 1987). This result is then in agreement with the potential chosen by Dzugutov. The reason why the first maximum is still well marked for $Al_{80}Ni_{20}$ stems from the strong contribution of the potential $\phi_{AlAl}(r)$. As for $Al_{80}Mn_{20}$ and $Al_{60}Mn_{40}$ the pair potential $\phi_{AlAl}(r)$ remains repulsive up to the second neighbours and it seems inherent in the Al-rich liquid alloys.

In the molecular dynamics simulations, the potentials used in the calculation of the instantaneous forces on each particle were truncated at distances r_t and smoothly damped down to zero at r_c with fifth-degree polynomials; (r_t, r_c) have been chosen equal to (4.3, 5.3), (4.5, 5.5) and (4.5, 5.7) (values in Å) for the AlAl, AlMn and MnMn pairs respectively. After 5×10^4 molecular dynamics time steps ($t_s = 1.5 \times 10^{-16}$ s) the system has attained its equilibrium, and 5×10^4 further steps were performed to sample different atomic configurations.

2.2. *Partial pair correlation functions and structure factors*

The partial pair correlation functions shown in figure 3 are the curves averaged over 50 equilibrium configurations taken among the last 5×10^4 steps at intervals of 10^3 steps. The overall agreement between the experimental curves (solid lines) and the calculated ones (dashed lines) is rather good. In particular, the two series of curves are well in phase in the whole r range. However, the first maxima of the calculated curves are always more intense. Nevertheless, since the following minima are also deeper, the numbers of first-nearest neighbours obtained by integration of the first peaks in the calculated curves are very close to the experimental values.

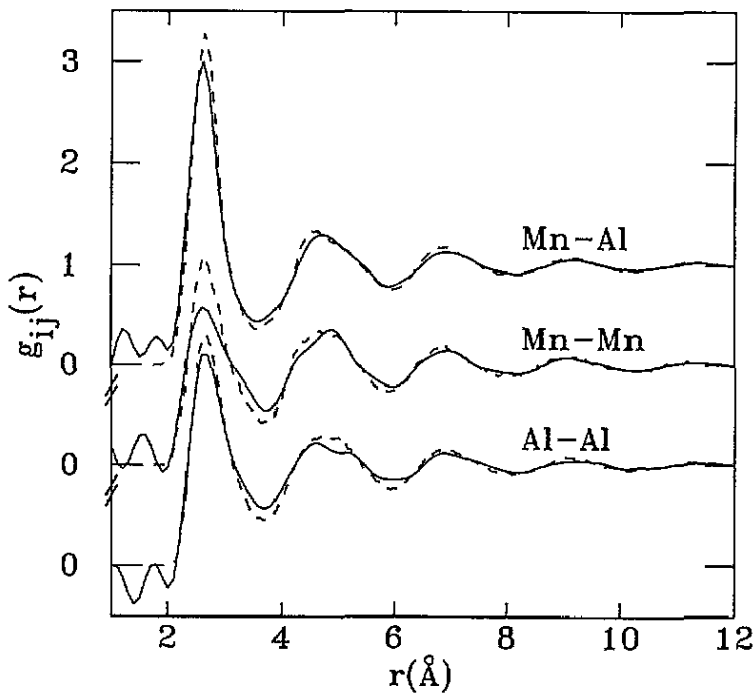

Figure 3. Partial correlation functions for liquid $Al_{60}Mn_{40}$: neutron diffraction (—) and molecular dynamics (- - -).

In figure 4, the MD Faber–Ziman partial structure factors, $I_{ij}(q)$, obtained by inverse Fourier transformation of the $g_{ij}(r)$ functions, fit the experimental curves reasonably well. The oscillations observed at low q are due to the limited size of the particle system. The comparison of the number–number structure factors, $S_{NN}(q)$, is presented in figure 5. The MD curve exhibits a sharper first peak and a second peak which is clearly split into two components at positions close to $1.7q_1$ and $2q_1$. The height ratio between the first peak and the component of the second peak at $1.7q_1$ remains similar to the experimental ratio equal to 0.4. As previously discussed (Maret *et al* 1991), this ratio deviates from the value found in the structure factor of an ideal curved-space icosahedral crystal described in a Ginzburg–Landau theory (Sachdev and Nelson 1984) equal to 0.49; let us recall that this ratio was exactly found for liquid $Al_{80}Mn_{20}$.

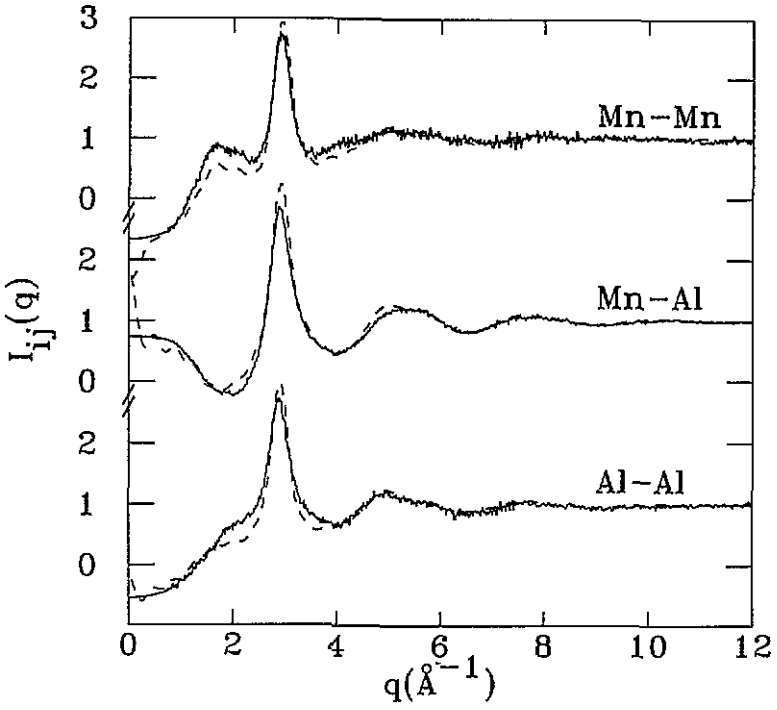

Figure 4. Faber–Ziman partial structure factors for liquid $Al_{60}Mn_{40}$: neutron diffraction (—) and molecular dynamics (- - -).

2.3. Local symmetries

The characterization of local symmetries and in particular that of icosahedral symmetry was realized in constructing around each particle its Voronoï cell (the polyhedron which contains all the points closer to this given particle than to any other). Each polyhedron is defined by a set of integers $(n_3, n_4, n_5,...)$ where n_i represents the number of faces having i edges and $\sum_i n_i$ defines a number of first neighbours around the central particle. The type of Voronoï polyhedron built around an atom having 12 nearest neighbours located at the vertices of an icosahedron is the pentagonal dodecahedron (0, 0, 12).

The Voronoï polyhedron statistics presented in table 1 were computed from 50 equilibrium configurations, the same as those used for the calculation of $g_{ij}(r)$ functions. For comparison, we also report the statistics, already published in paper I, found in the MD configurations of liquid $Al_{80}Mn_{20}$ and in an AlMnSi relaxed icosahedral quasicrystal model which is in good agreement with the pair correlation functions measured in the $Al_{74}Si_5Mn_{21}$ icosahedral phase (Lançon and Billard 1990). Among the 12 most frequently occurring types of Voronoï polyhedron, 11 are common to the two liquids and the two remaining ones have close percentages. This indicates that the well developed topological ordering in these AlMn alloys, characterized by a sharp first peak in their $S_{NN}(q)$ function, is grounded on the same kinds of local symmetry since at least 28% of sites in the MD configurations have identical symmetry.

Now, let us compare with the three polyhedron types found in the nearest stable compound of rhombohedral γ-Al_8Cr_5-type structure from the liquid composition $Al_{60}Mn_{40}$, which are (0, 4, 4, 7), (1, 0, 9, 3) and (0, 1, 10, 2) occurring with the following percentages: 46%, 31% and 23% respectively. We have found that only 5.6% of the atomic sites in the

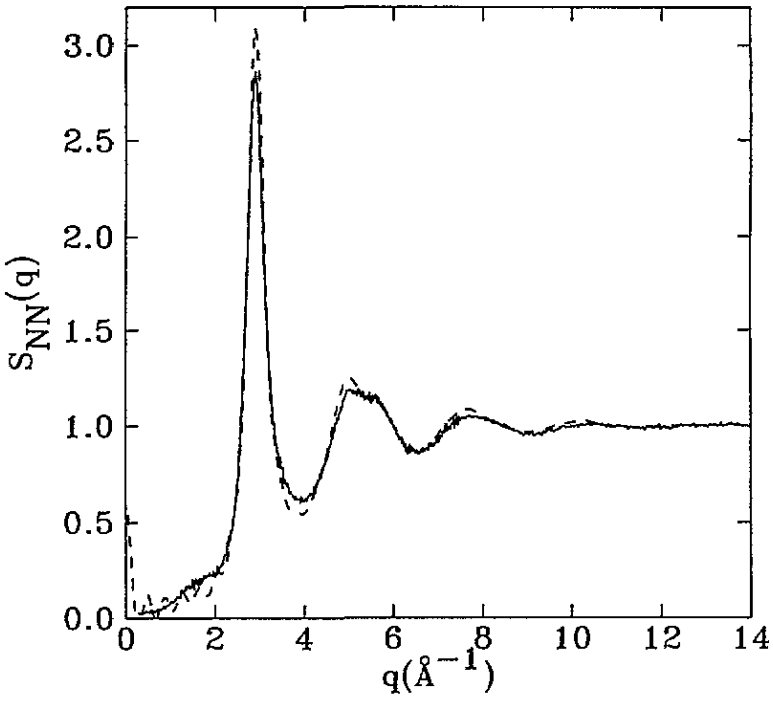

Figure 5. Number–number structure factor for liquid $Al_{60}Mn_{40}$: neutron diffraction (—) and molecular dynamics (- - -).

Table 1. Types and percentages of the most frequent Voronoï polyhedra in the equilibrium configurations of $Al_{60}Mn_{40}$ generated by molecular dynamics. For comparison we also report the results obtained in the equilibrium MD configurations of liquid $Al_{80}Mn_{20}$ and in a relaxed icosahedral quasicrystal model of AlMnSi, previously presented in paper I.

Liquid $Al_{80}Mn_{20}$ MD		Liquid $Al_{60}Mn_{40}$ MD		Quasicrystal model	
$(n_3, n_4, n_5, \ldots)$	%	$(n_3, n_4, n_5, \ldots)$	%	$(n_3, n_4, n_5, \ldots)$	%
(0, 3, 6, 4)	4.1 ± 0.2	(0, 3, 6, 4)	4.8 ± 0.3	(0, 3, 6, 6)	7.1
(0, 1, 10, 2)	4.1 ± 0.2	(0, 2, 8, 4)	4.1 ± 0.2	(0, 3, 6, 5)	6.2
(0, 2, 8, 4)	3.8 ± 0.2	(0, 1, 10, 2)	3.8 ± 0.3	(0, 2, 8, 4)	5.8
(0, 2, 8, 2)	2.8 ± 0.2	(0, 3, 6, 5)	2.7 ± 0.2	(0, 0, 12)	5.6
(0, 0, 12)	2.3 ± 0.2	(0, 2, 8, 2)	2.7 ± 0.2	(0, 4, 4, 7)	3.1
(0, 3, 6, 5)	2.0 ± 0.2	(0, 4, 4, 6)	1.8 ± 0.2	(0, 3, 6, 4)	2.8
(0, 1, 10, 3)	1.8 ± 0.2	(1, 3, 4, 5, 1)	1.8 ± 0.2	(0, 1, 10, 3)	2.7
(0, 2, 8, 5)	1.7 ± 0.2	(0, 2, 8, 5)	1.7 ± 0.1	(0, 2, 8, 5)	2.6
(0, 3, 6, 3)	1.6 ± 0.2	(0, 2, 8, 3)	1.7 ± 0.2	(0, 4, 4, 8)	2.5
(0, 2, 8, 3)	1.6 ± 0.2	(0, 1, 10, 3)	1.7 ± 0.2	(0, 1, 10, 2)	2.5
(1, 2, 6, 3, 1)	1.5 ± 0.1	(0, 0, 12)	1.7 ± 0.2	(0, 2, 8, 1)	2.1
(1, 3, 4, 5, 1)	1.4 ± 0.1	(1, 2, 6, 3, 1)	1.6 ± 0.2	(1, 2, 6, 2, 1)	2.1
...	...	...	...		
(0, 4, 4, 6)	1.3 ± 0.1	(0, 3, 6, 3)	1.5 ± 0.2		

simulated liquid $Al_{60}Mn_{40}$ present these symmetries. It is interesting to recall that only two types of polyhedron found in the cubic α-AlMnSi phase were also found in the MD configurations of liquid $Al_{80}Mn_{20}$ representing 6.1% of atomic sites.

Finally, the conclusions which can be drawn from this analysis are the following ones:

(i) On the one hand, the most frequent types of local symmetry found in the molecular dynamics configurations of liquid $Al_{60}Mn_{40}$ and $Al_{80}Mn_{20}$ are roughly the same ones. Moreover, they are more specific to the icosahedral quasicrystal model than to the stable crystalline phases of close composition, since at least 17% of the atomic sites in both liquids have the same type of local symmetry as in the quasicrystal model.

(ii) On the other hand, there are slightly fewer atomic sites with icosahedral symmetry in the non-quasicrystal-forming $Al_{60}Mn_{40}$ liquid than in the liquid $Al_{80}Mn_{20}$.

3. Reverse Monte Carlo simulations of liquid $Al_{60}Mn_{40}$ and $Al_{71}Pd_{19}Mn_{10}$

In paper I, we have shown that the RMC simulations of liquid $Al_{80}Mn_{20}$ lead to configurations in perfect agreement with experiment and in which the most frequent types of Voronoï polyhedron are roughly the same as those in the molecular dynamics configurations but with lower percentages. From these results, it was concluded that the RMC configurations were more disordered than those generated by molecular dynamics.

However the RMC configurations were well described by the experimental pair correlation functions while the functions $g_{ij}(r)$ characterizing the MD configurations were somewhat different from the experimental ones especially in the first peak intensities. So to figure out whether the difference in the local environments obtained from the two methods can be explained by the differences in their $g_{ij}(r)$ functions or come intrinsically from the methods themselves, we will also compare RMC and MD configurations which both are described by the same $g_{ij}(r)$ functions. To obtain these RMC configurations, RMC simulations have been done to fit the $g_{ij}(r)$ curves obtained by molecular dynamics and not the experimental ones.

In this section, we first present the results of RMC simulations for the binary $Al_{60}Mn_{40}$ liquid alloy, previously modelled by molecular dynamics (section 2.1), using different sets of partial pair correlation functions for the standard χ^2 test (the experimental or the MD curves) and also different initial configurations. From these results, the sensitivity of the RMC method to the simulation conditions will be discussed. Then, we present the results obtained by this technique for the ternary liquid alloy $Al_{71}Pd_{19}Mn_{10}$, based on the partial function $g_{MnMn}(r)$ and two combinations of the other five partial pair correlation functions.

3.1. Liquid $Al_{60}Mn_{40}$

The reverse Monte Carlo method has been described by McGreevy and Pusztai (1988). Here we just give a brief summary and the main parameters which govern the simulations. In this technique, a new configuration is generated by random motion of one particle with a maximal displacement equal to 0.1 Å for the two species. If the particle in motion approaches any other particle within a distance smaller than r_{ij}^0, the new configuration is automatically rejected. Otherwise, the new pair correlation functions $g_{ij}'(r)$ describing the new configuration are compared to the curves $g_{ij}^E(r)$ to be fitted, using a standard χ^2 test such as

$$\chi'^2 = \sum_{ij} \sum_{k=1}^{n} \frac{(g_{ij}^E(r_k) - g_{ij}'(r_k))^2}{\sigma_{ij}^2}. \tag{4}$$

n is the number of data points and σ_{ij} are the errors in the curves of reference equal to 0.02 Å in the whole r range. If $\chi'^2 < \chi^2$ (χ^2 being the value for the previous configuration), the

new configuration is accepted; if $\chi'^2 > \chi^2$, it is accepted with a probability that follows a normal distribution. The process is repeated until χ^2 becomes stable around an equilibrium value. The size of the particle system is identical to that chosen in molecular dynamics. Two initial configurations were chosen: the first one is the final configuration obtained by MD and the second one is a random configuration with the same minimal interatomic distances, r_{ij}^0, as those used in MD.

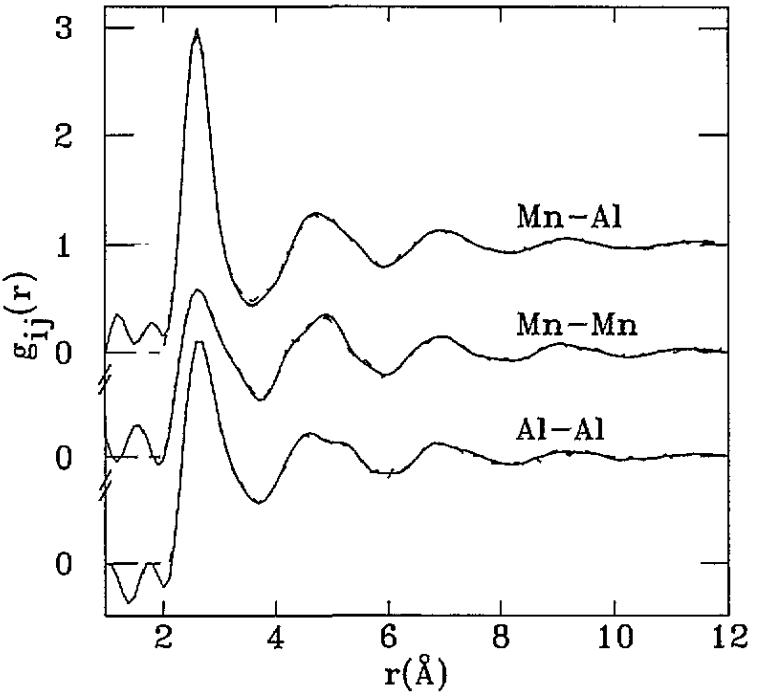

Figure 6. Partial correlation functions for liquid $Al_{60}Mn_{40}$: neutron diffraction (—) and reverse Monte Carlo fit (- - -), see also text.

Figures 6 and 7 show the calculated RMC $g_{ij}(r)$ curves (dashed lines) which are in excellent agreement with the driving functions in the RMC simulations, namely the experimental curves (solid lines in figure 6) and the MD curves (solid lines in figure 7), in both cases starting from a random configuration. The RMC curves in figure 6 and 7 are calculated in the last equilibrium configuration obtained after 4×10^5 and 6×10^6 accepted moves respectively, but the corresponding χ^2 values have already attained their minimal values after roughly half of these numbers.

The $S_{NN}(q)$ function derived from the $I_{ij}(q)$ functions, obtained by Fourier transformation of the RMC curves presented in figure 6, is compared with the experimental function in figure 8. The agreement in the whole q range is very good, especially in the region of the second peak which suggests a good description of icosahedral local order in the RMC configurations.

The local symmetries in the RMC equilibrium configurations generated using different initial configurations or curves of reference are again analysed via the construction of the Voronoï polyhedra. In table 2, we present the Voronoï polyhedron statistics computed in the RMC configurations which are consistent, either with the MD curves referred to RMC-1 starting from the final MD configuration and RMC-2 starting from a random configuration,

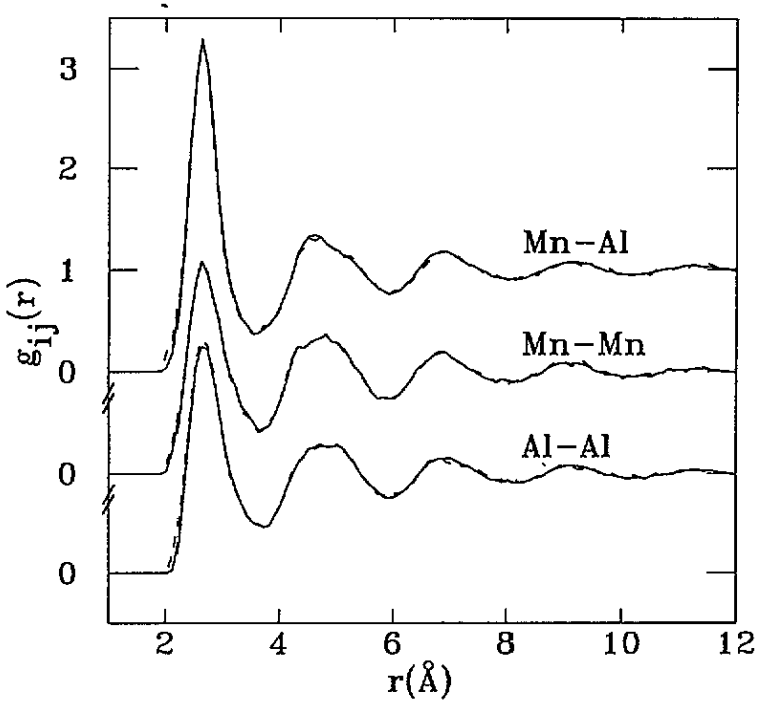

Figure 7. Partial correlation functions for liquid $Al_{60}Mn_{40}$: molecular dynamics (—) and reverse Monte Carlo fit (- - -), see also text.

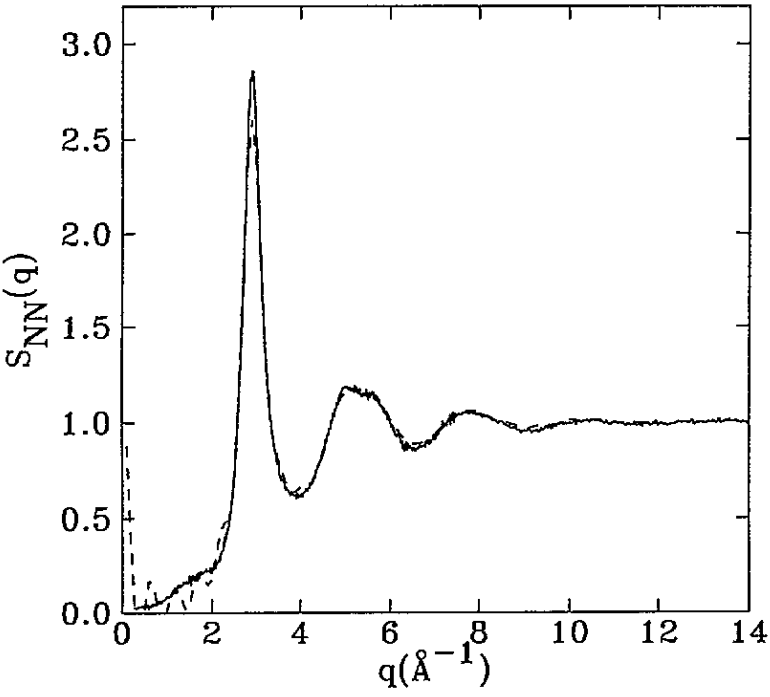

Figure 8. Number–number structure factor for liquid $Al_{60}Mn_{40}$: neutron diffraction (—) and reverse Monte Carlo fit (- - -).

or with the experimental curves referred to RMC-3 starting from a random configuration. For comparison with the MD simulations, we give again the results presented in table 1 for $Al_{60}Mn_{40}$. The percentages of the most frequently occurring types of polyhedron are the

values averaged over 18, 12 and nine equilibrium configurations for the simulations RMC-1, RMC-2 and RMC-3 respectively, the corresponding 1% confidence intervals are consequently broader than those calculated in the 50 MD equilibrium configurations. The comparison of these four statistics leads to the following remarks.

(i) When the RMC simulations are based on the MD curves, the most frequent types of polyhedron found in the corresponding RMC configurations are identical to those in the MD configurations and within their 1% confidence intervals they appear with roughly the same frequencies.

(ii) In the same way, the comparison of the RMC-1 and RMC-2 results indicates that the occurrence frequencies of the polyhedra are roughly independent of the initial values. However, for the Voronoï polyhedra having a large number of pentagonal faces such as (0, 1, 10, 2), (0, 1, 10, 3) and (0, 0, 12), their percentages in the final configurations seem somewhat dependent on their values in the initial states. These initial values are equal to 4.3, 2.1 and 1.4 respectively for RMC-1 (values of the molecular dynamics final configuration) and are equal to 0.5, 0.5 and 0 for RMC-2 (values in a random configuration). Such behaviour was also observed for liquid $Al_{80}Mn_{20}$ in the RMC configurations obtained by fitting the experimental $g_{ij}(r)$ functions; the percentages of the polyhedra (0, 1, 10, 2) and (0, 0, 12) decreased from 2.2 to 1.6 and from 1 to 0.5 respectively when changing the initial configuration from the final MD configuration to a random configuration.

(iii) The influence of the reference functions $g_{ij}^{E}(r)$ used in the RMC simulations is illustrated by the comparison of the RMC-2 and RMC-3 results. Among the eleven most frequent types of polyhedron given in table 2, eight are common to the simulations RMC-2 and RMC-3; however the percentages obtained using the experimental functions are systematically lower than those using the MD curves. This shows that local order, in particular the icosahedral symmetry, is very sensitive to the choice of the $g_{ij}(r)$ functions.

The comparison of the RMC results between the two liquids $Al_{80}Mn_{20}$ and $Al_{60}Mn_{40}$ is presented in section 3.3, together with those obtained for the ternary alloy $Al_{71}Pd_{19}Mn_{10}$.

3.2. *Liquid $Al_{71}Pd_{19}Mn_{10}$*

A complete description of the structure of a ternary alloy requires the determination of six partial structure factors. Up to now, such a separation was never achieved since it necessitates, on the one hand, the isomorphic or isotopic substitution of two elements, and on the other hand, measurements of total structure factors with an accuracy better than 0.001. The neutron diffraction measurements in the $Al_{71}Pd_{19}[Mn_y(FeCr)_{1-y}]_{10}$ liquid alloys based on a single substitution between Mn atoms and the equiatomic FeCr mixture have not allowed us to separate the contributions of the Al and Pd atoms (Maret *et al* 1993a). From the three total stucture factors measured with y=1, 0.64 and 0 we were able to determine the partial function $I_{MnMn}(q)$ and two combinations of the other partial functions $I_{AA}(q)$ and $I_{MnA}(q)$ in a pseudo-binary description $A_{90}Mn_{10}$ (A=Al or Pd) given by

$$I_{AA}(q) = [c_{Al}^2 b_{Al}^2 I_{AlAl}(q) + 2c_{Al}c_{Pd}b_{Al}b_{Pd}I_{AlPd}(q) + c_{Pd}^2 b_{Pd}^2 I_{PdPd}(q)]/c_A^2 b_A^2 \quad (5)$$

$$I_{MnA}(q) = [c_{Al}b_{Al}I_{MnAl}(q) + c_{Pd}b_{Pd}I_{MnPd}(q)]/c_A b_A \quad (6)$$

with $c_A = c_{Al} + c_{Pd}$ and $b_A = (c_{Al}b_{Al} + c_{Pd}b_{Pd})/c_A$; c_i and b_i are the atomic concentration and the coherent scattering length of species i. The same relations hold for the $g_{AA}(r)$ and $g_{MnA}(r)$ functions.

The RMC simulations of liquid $Al_{71}Pd_{19}Mn_{10}$ are then based on these two latter functions and the partial $g_{MnMn}(r)$. The particle system consists of 613 Al atoms, 164 Pd atoms and

Table 2. Comparison of the Voronoï polyhedron statistics computed in liquid configurations of $Al_{60}Mn_{40}$ obtained from molecular dynamics (MD) and reverse Monte Carlo fits based either on the MD curves starting from the final MD configuration (RMC-1) or from a random configuration (RMC-2), or on the experimental curves starting from a random configuration (RMC-3).

Liquid $Al_{60}Mn_{40}$ MD		Liquid $Al_{60}Mn_{40}$ RMC-1	
$(n_3, n_4, n_5, \ldots)$	%	$(n_3, n_4, n_5, \ldots)$	%
(0, 3, 6, 4)	4.8 ± 0.3	(0, 2, 8, 4)	5.0 ± 0.5
(0, 2, 8, 4)	4.1 ± 0.2	(0, 1, 10, 2)	4.9 ± 0.4
(0, 1, 10, 2)	3.8 ± 0.3	(0, 3, 6, 4)	4.5 ± 0.4
(0, 3, 6, 5)	2.7 ± 0.2	(0, 3, 6, 5)	3.7 ± 0.5
(0, 2, 8, 2)	2.7 ± 0.2	(0, 1, 10, 3)	2.5 ± 0.3
(0, 4, 4, 6)	1.8 ± 0.2	(0, 4, 4, 6)	2.2 ± 0.2
(1, 3, 4, 5, 1)	1.8 ± 0.2	(0, 2, 8, 2)	2.2 ± 0.3
(0, 2, 8, 5)	1.7 ± 0.1	(0, 0, 12)	2.1 ± 0.2
(0, 2, 8, 3)	1.7 ± 0.2	(1, 3, 4, 5, 1)	2.0 ± 0.3
(0, 1, 10, 3)	1.7 ± 0.2	(0, 2, 8, 3)	2.0 ± 0.4
(0, 0, 12)	1.7 ± 0.2	(0, 2, 8, 5)	2.0 ± 0.3
...	...	...	...

Liquid $Al_{60}Mn_{40}$ RMC-2		Liquid $Al_{60}Mn_{40}$ RMC-3	
$(n_3, n_4, n_5, \ldots)$	%	$(n_3, n_4, n_5, \ldots)$	%
(0, 3, 6, 4)	5.9 ± 0.9	(0, 3, 6, 4)	3.8 ± 0.6
(0, 2, 8, 4)	4.8 ± 0.8	(0, 2, 8, 4)	2.2 ± 0.7
(0, 1, 10, 2)	4.4 ± 0.7	(0, 3, 6, 5)	2.2 ± 0.5
(0, 3, 6, 5)	3.3 ± 0.6	(0, 4, 4, 6)	1.8 ± 0.5
(0, 4, 4, 6)	2.6 ± 0.5	(1, 3, 4, 5, 1)	1.7 ± 0.5
(0, 2, 8, 3)	2.3 ± 0.6	(1, 2, 6, 3, 1)	1.5 ± 0.4
(1, 3, 4, 5, 1)	2.2 ± 0.4	(0, 2, 8, 2)	1.5 ± 0.5
(0, 2, 8, 5)	2.2 ± 0.5	(0, 3, 6, 3)	1.5 ± 0.5
(0, 3, 6, 6)	2.0 ± 0.5	(0, 2, 8, 3)	1.4 ± 0.4
(0, 2, 8, 2)	1.8 ± 0.4	(0, 3, 6, 6)	1.3 ± 0.3
(0, 1, 10, 3)	1.8 ± 0.4	(1, 3, 5, 3, 2)	1.3 ± 0.4
...	...	...	...
		(0, 1, 10, 2)	1.2 ± 0.4
(0, 0, 12)	1.6 ± 0.4	(0, 0, 12)	0.3 ± 0.2

87 Mn atoms contained in a cubic box of length 24.9 Å such that its atomic density is that of the liquid equal to 0.056 atoms $Å^{-3}$. In the initial configuration, the particles are randomly distributed with the constraint of a minimal distance equal to 2.2 Å for all the atomic pairs, except that for the MnMn pairs, equal to 3 Å; the latter value, chosen in agreement with experiment, indicates the absence of MnMn contacts in liquid $Al_{71}Pd_{19}Mn_{10}$. The maximal displacement is 0.1 Å for all the particles and the errors in the experimental functions, constant in the whole r range, are equal to 0.02, 0.04 and 0.1 for the pairs AA, MnA and MnMn respectively.

The RMC curves shown in figure 9 (dashed lines) are calculated in a single equilibrium configuration obtained after 1.3×10^6 accepted moves; the value of χ^2 has attained its equilibrium value after roughly 8×10^5 accepted displacements. In comparison with $Al_{60}Mn_{40}$ the convergence is significantly lower. For the $g_{MnAl}(r)$ and $g_{AA}(r)$ functions the agreement between experiment and reverse Monte Carlo is excellent and that for $g_{MnMn}(r)$ is rather satisfactory. The deviation observed in the first maximum of $g_{MnMn}(r)$ corresponds to a number of missing MnMn first pairs equal to 0.3 from a total number of 2.9. The

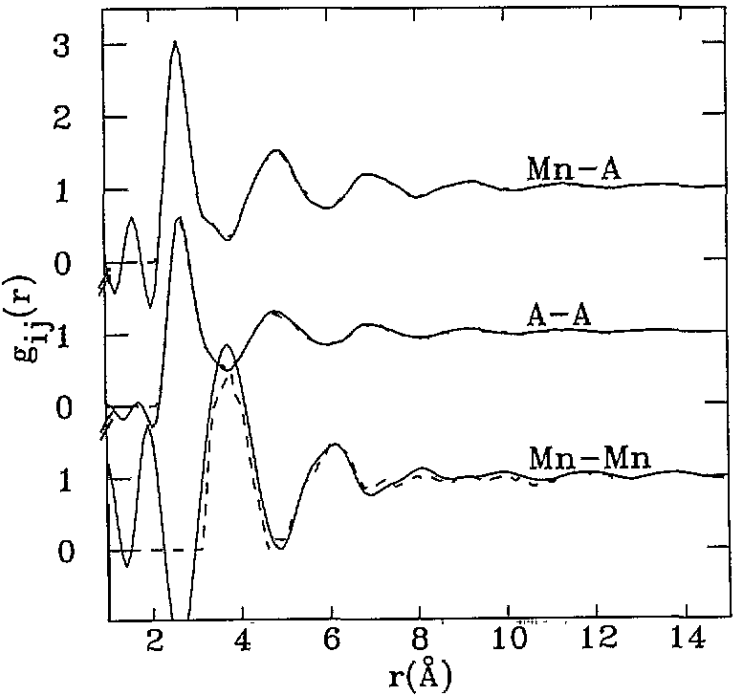

Figure 9. Partial correlation functions of liquid $Al_{71}Pd_{19}Mn_{10}$ in a pseudo-binary $A_{90}Mn_{10}$ (A = Al or Pd) description: neutron diffraction (—) and reverse Monte Carlo fit (- - -).

use of a coordination constraint on these pairs has not allowed us to improve the fit of $g_{MnMn}(r)$. The standard deviation in the experimental $g_{MnMn}(r)$ function, chosen equal to 0.1, is an optimized value in order to limit the data dispersion in the RMC curve. In fact, the experimental error in the partial structure factor $I_{MnMn}(q)$ is at least 50%, therefore a moderate agreement for the MnMn pairs should not be surprising.

Figure 10 shows the agreement between the experimental total structure factors and the RMC curves calculated as follows:

$$I(q) = [c_A^2 b_A^2 I_{AA}(q) + 2c_A c_{Mn} b_A b_{Mn} I_{MnA}(q) + c_{Mn}^2 b_{Mn}^2 I_{MnMn}(q)]/\langle b\rangle^2 \quad (7)$$

where $\langle b\rangle = c_A b_A + c_{Mn} b_{Mn}$ and $I_{ij}(q)$ are the Fourier transforms of the RMC $g_{ij}(r)$ curves. As mentioned in the introduction the structure factor for y=0.25 is a good measurement of the number–number structure factor; the overall agreement between the calculated and experimental curves means that the topological ordering in these ternary alloys would be well described in the RMC configurations in spite of the deviations observed in the MnMn distribution. Therefore, the characterization of local symmetries via the construction of the Voronoï polyhedra can be applied to the ternary alloy $Al_{71}Pd_{19}Mn_{10}$.

3.3. Discussion

The statistics of the Voronoï polyhedra in liquid $Al_{71}Pd_{19}Mn_{10}$ were computed in 14 equilibrium configurations taken among the last 4×10^5 steps (table 3). For a clear comparison, we also present the results of the RMC simulations for the binary liquid $Al_{80}Mn_{20}$ and we recall the RMC-3 results for $Al_{60}Mn_{40}$. All results are based on the experimental pair correlation functions and use random configurations as starting points.

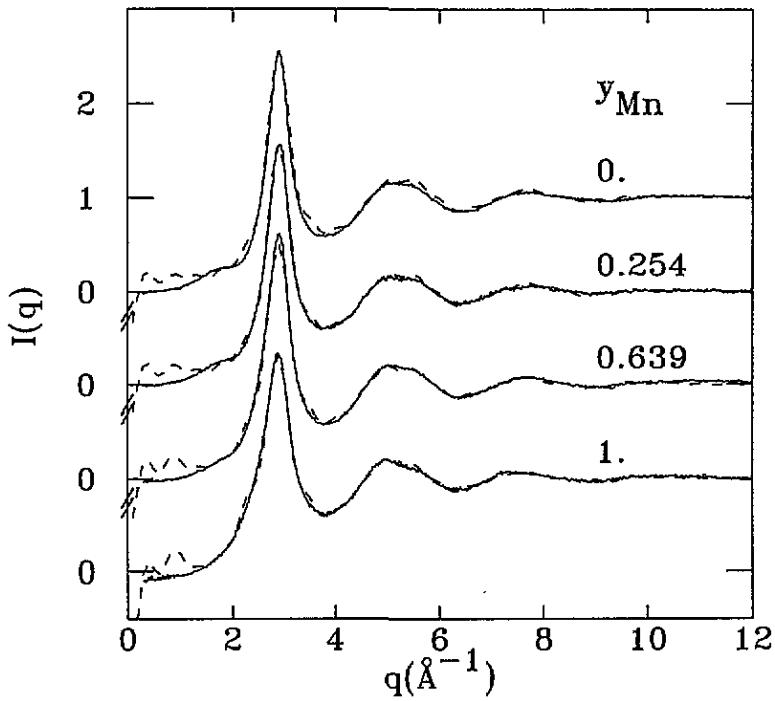

Figure 10. Total structure factors for liquid $Al_{71}Pd_{19}[Mn_y(FeCr)_{1-y}]_{10}$: neutron diffraction (—) and reverse Monte Carlo fit (- - -). Note that above 2 Å^{-1} the function for $y = 0.254$ is very close to the number–number structure factor.

Table 3. Comparison of the Voronoï polyhedron statistics in liquid $Al_{80}Mn_{20}$, $Al_{71}Pd_{19}Mn_{10}$ and $Al_{60}Mn_{40}$ calculated in the equilibrium configurations generated by reverse Monte Carlo simulations starting from a random configuration.

Liquid $Al_{80}Mn_{20}$ RMC		Liquid $Al_{71}Pd_{19}Mn_{10}$ RMC		Liquid $Al_{60}Mn_{40}$ RMC-3	
$(n_3, n_4, n_5, \ldots)$	%	$(n_3, n_4, n_5, \ldots)$	%	$(n_3, n_4, n_5, \ldots)$	%
(0, 3, 6, 4)	3.2 ± 0.2	(0, 3, 6, 4)	2.7 ± 0.6	(0, 3, 6, 4)	3.8 ± 0.6
(0, 2, 8, 4)	2.4 ± 0.2	(0, 2, 8, 2)	1.7 ± 0.4	(0, 2, 8, 4)	2.2 ± 0.7
(0, 3, 6, 5)	1.9 ± 0.3	(0, 2, 8, 4)	1.6 ± 0.4	(0, 3, 6, 5)	2.2 ± 0.5
(0, 2, 8, 2)	1.9 ± 0.3	(0, 1, 10, 2)	1.5 ± 0.4	(0, 4, 4, 6)	1.8 ± 0.5
(0, 1, 10, 2)	1.6 ± 0.3	(1, 3, 4, 5, 1)	1.4 ± 0.4	(1, 3, 4, 5, 1)	1.7 ± 0.5
(1, 3, 4, 5, 1)	1.5 ± 0.2	(1, 2, 6, 3, 1)	1.4 ± 0.4	(1, 2, 6, 3, 1)	1.5 ± 0.4
(0, 3, 6, 3)	1.5 ± 0.2	(0, 3, 6, 3)	1.3 ± 0.3	(0, 2, 8, 2)	1.5 ± 0.5
(1, 2, 6, 3, 1)	1.5 ± 0.3	(0, 3, 6, 5)	1.3 ± 0.3	(0, 3, 6, 3)	1.5 ± 0.5
(0, 4, 4, 6)	1.3 ± 0.2	(1, 3, 4, 4, 1)	1.1 ± 0.4	(0, 2, 8, 3)	1.4 ± 0.4
(0, 4, 5, 4, 1)	1.3 ± 0.2	(0, 4, 5, 4, 1)	1.1 ± 0.3	(0, 3, 6, 6)	1.3 ± 0.3
	...	...	...	...	...
				(0, 1, 10, 2)	1.2 ± 0.4
(0, 0, 12)	0.5 ± 0.2	(0, 0, 12)	0.6 ± 0.2	(0, 0, 12)	0.3 ± 0.2

First, the comparison between $Al_{80}Mn_{20}$ and $Al_{71}Pd_{19}Mn_{10}$ shows that the eight most frequent polyhedra are identical and the percentages of those characterizing icosahedral symmetry, (0, 0, 12) and (0, 1, 10, 2), are very close. These points indicate quite clearly that the two liquids exhibit similar topological ordering, previously suggested from the

superimposition of their experimental function $S_{NN}(q)$ drawn as a function of q/q_1 (Maret *et al* 1993a).

The comparison of the results between the two binary alloys $Al_{80}Mn_{20}$ and $Al_{60}Mn_{40}$ leads to the same conclusions as those drawn in section 2.1 from the molecular dynamics simulations. Among the ten most frequent types of polyhedron, eight are common to the two liquids; this confirms that their topological ordering is mainly based on the same types of local symmetry.

4. Conclusions

Both molecular dynamics and reverse Monte Carlo simulations have shown that topological ordering in liquid $Al_{80}Mn_{20}$ and $Al_{60}Mn_{40}$ is mainly formed by the same types of local symmetry. A slight decrease of the icosahedral symmetry is observed in liquid $Al_{60}Mn_{40}$.

The RMC simulations of the ternary liquid $Al_{71}Pd_{19}Mn_{10}$ lead to configurations in good agreement with the experimental pair correlation functions, $g_{AA}(r)$, $g_{MnA}(r)$ and $g_{MnMn}(r)$, in a pseudo-binary $A_{90}Mn_{10}$ description. It is remarkable that the eight most commonly occurring types of Voronoï polyhedron are identical to those observed in the RMC liquid configurations of $Al_{80}Mn_{20}$. These RMC simulations then confirm the similarity between the topological orders in liquid $Al_{71}Pd_{19}Mn_{10}$ and $Al_{80}Mn_{20}$, previously suggested from the comparison of their number–number structure factor.

In a general way, the reverse Monte Carlo method is a powerful method coupled with the construction of Voronoï polyhedra for characterizing the local symmetries in disordered materials. However, for a given system, the analysis of the occurrence frequencies of the polyhedra should always be done in comparison with other structurally close systems and if possible with other simulation methods such as molecular dynamics.

Acknowledgments

We would like to acknowledge Dr M A Howe and Dr R L McGreevy for providing the reverse Monte Carlo programs.

References

Dzugutov M 1992 *Phys. Rev.* A **46** R2984
Hoover H G, Ladd A J C and Moran B 1982 *Phys. Rev. Lett.* **48** 1818
Lançon F and Billard L 1990 *J. Physique* **51** 1099
Maret M, Chieux P, Dubois J M and Pasturel A 1991 *J. Phys.: Condens. Matter* **3** 2801
Maret M, Dubois J M and Chieux P 1993a *J. Non-Cryst. Solids* **156–158** 918
Maret M, Lançon F and Billard L 1993b *J. Physique* I **3** 1873
Maret M, Pomme T, Pasturel A and Chieux P 1990 *Phys. Rev.* B **42** 1598
Matthai C C and March N H 1982 *Phys. Chem. Liq.* **11** 207
McGreevy R L and Pusztai L 1988 *Mol. Simul.* **1** 359
Sachdev S and Nelson D R 1984 *Phys. Rev. Lett.* **53** 1947
Sadoc J F and Mosseri R 1987 *Extended Icosahedral Structures* ed M Jaric and D Gratias (New York: Academic)
Tsai A, Inoue A, Yokoyama Y and Masumoto T 1990 *Phil. Mag. Lett.* **61** 9